HHS Public Access

Author manuscript

Bioconjug Chem. Author manuscript; available in PMC 2017 August 15.

Published in final edited form as:

Bioconjug Chem. 2017 February 15; 28(2): 649–658. doi:10.1021/acs.bioconjchem.6b00708.

Detecting Chronic Post-Traumatic Osteomyelitis of Mouse Tibia via an IL-13Rα2 Targeted Metallofullerene Magnetic Resonance Imaging Probe

Li Xiao[†,#], **Tinghui Li**[‡,#], **Mengmeng Ding**[†], **Jiezuan Yang**[†], **José Rodríguez-Corrales**[‡], **Stephen M. LaConte**[‖], **Nicholas Nacey**[§], **David B. Weiss**[†], **Li Jin**[†], **Harry C. Dorn**[*,‡,‖], and **Xudong Li**[*,†]

[†]Department of Orthopaedic Surgery, University of Virginia, Charlottesville, Virginia 22908, United States

[§]Department of Radiology and Medical Imaging, University of Virginia, Charlottesville, Virginia 22908, United States

[‖]Virginia Tech Carilion Research Institute, Roanoke, Virginia 24016, United States

[‡]Department of Chemistry, Virginia Polytechnic Institute and State University, Blacksburg, Virginia 24061, United States

Abstract

Differential diagnosis of chronic post-traumatic osteomyelitis (CPO) from aseptic inflammation remains challenging, since both pathological processes share similar clinical symptoms. Here we utilized a novel targeted metallofullerene nanoparticle based magnetic resonance imaging (MRI) probe IL-13-TAMRA-$Gd_3N@C_{80}(OH)_{30}$− $(CH_2CH_2COOH)_{20}$ to detect CPO in mouse tibia via overexpressed IL-13Rα2 receptors. The functionalized metallofullerene was characterized by X-ray photoelectron spectroscopy. Upon lipopolysaccharide (LPS) stimulation, macrophage Raw 264.7 cells showed elevated IL-13Rα2 expression via immunofluorescence staining and increased MRI probe binding via built-in TAMRA fluorescence imaging. Trauma was induced in both tibia of mice and bacteria soaked suture was inserted into the right tibia to initiate infection. During the acute phase (1.5 weeks), luminol-bioluminescence imaging revealed much higher myeloperoxidase activity in the infected tibia compared to the sham. In the chronic phase (4 weeks), X-ray radiography illustrated bone deformation in the infected tibia compared to the sham. With T_1 weighted sequences, the probe clearly exhibited hyperintensity in the infection foci at both acute and chronic phases, which was not observed in the sham tibia. Histological analysis revealed severe bone structural destruction and massive inflammatory cell infiltration in the infected tibia. Immunohistochemistry confirmed abundant expression of IL-13Rα2 in the infection

[*]**Corresponding Authors:** hdorn@vt.edu. Tel: 540-526-2049. xl2n@virginia.edu. Tel: 434-982-4135. Fax: 434-924-1691.
[#]Author Contributions: These authors contributed equally to the current work.

Supporting Information

The Supporting Information is available free of charge on the ACS Publications website at DOI: 10.1021/acs.bioconj-chem.6b00708. Additional in vitro and in vivo characterization data of this MRI probe (PDF)

Notes

The authors declare no competing financial interest.

site. In summary, we developed a noninvasive imaging approach to detect and differentiate CPO from aseptic inflammation using a new IL-13Rα2 targeted metallofullerene MRI probe. In addition, for the first time, IL-13Rα2 was investigated as a unique biomarker in the context of osteomyelitis. Our data established a foundation for the translational application of this MRI probe in the clinical differentiation of CPO.

Graphical abstract

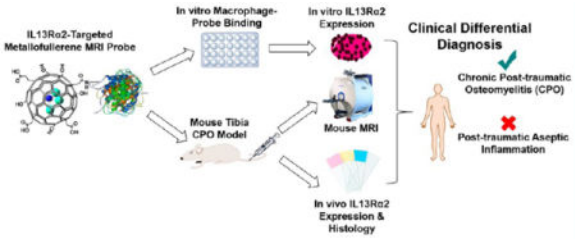

INTRODUCTION

Osteomyelitis is an infection of the bone marrow and adjacent bone typically caused by *Staphylococcus aureus* (*S. aureus*), which is associated with high levels of inflammation and bone tissue destruction.[1] Chronic post-traumatic osteomyelitis (CPO) can develop through contiguous spread from a local or circulating infective pathogens after trauma, bone surgery, or joint replacement.[2] The average rate of post-traumatic infection in open tibia fractures is approximately 10%.[3] In addition, the dramatically increased number of joint replacement procedures has been associated with increased incidents of infection, and is projected to increase over the next 15 years.[4] Chronic osteomyelitis is painful and debilitating and is associated with considerable morbidity, and may be limb-threatening.[5] Consequently, the rate of clinical failure in osteomyelitis treatment is high, and frequently results in loss of function and/or amputation.[6] Therefore, prompt and accurate diagnosis is extremely critical to early intervention and positive clinical outcome.

Unfortunately, clinical differential diagnosis of CPO from aseptic inflammation remains challenging, since many early signs of infection are similar to sterile (asepsis) inflammatory reactions following trauma or surgery. Bone culture remains the gold standard of diagnosis; however, high false-negative rates of ~40% has been reported.[7–9] Although computed tomography (CT) can delineate lesions in the medullary canal and inflammation in the soft tissues, the presence of other pathological processes, such as stress fractures, osteoid osteomas, and benign tumor, may confound the diagnosis.[10] Nuclear medicine such as ^{99m}Tc-methylene diphosphonate (^{99m}Tc-MDP), ^{18}F-fluorodeoxyglucose (FDG), or radiolabeled white blood cells (WBC) has shown high sensitivity to track inflammatory activities associated with infection; nevertheless, these methods still suffer from the aforementioned issues.[10–12]

In recent years, research efforts have shifted to develop targeted imaging probes for various modalities. Peptide, proteins, or nanoparticles have been chemically synthesized to be optical, nuclear, and MRI imaging probes. In general, optical imaging is preferable in the

research setting with limited clinical potential.[13,14] Nuclear imaging has high sensitivity and specificity;[15–17] however, its clinical application might be impeded by laborious synthetic procedures, limited shelf life of radio-isotopes, and narrow detection window following probe administration. Targeted MRI appears to be a favored choice as it not only provides excellent imaging contrast and resolution, but also allows detection of biological response at functional or even molecular level without employing ionizing radiation.[18] Recently, superparamagnetic iron oxide nano-particles (SPIONs) have been utilized as contrast agents for in vivo MRI detection of infiltrated macrophages to identify infection in patients with septic arthritis and osteomyelitis, given to the phagocytosis by macrophages after probe administration.[19,20] This is because the persistence of the pathogenic agents during the chronic stage of osteomyelitis leads to constant recruitment of macrophages to the site of infection, resulting in macrophages as the most abundant immune cells in the infection foci, unlike aseptic inflammation.[21,22] Although macrophage phagocytosis contributes to the detection of most nanoparticle-based imaging probes, this mechanism still relies on a passive uptake. Thus, receptor-mediated targeted MRI imaging using functionalized nanoparticles would be more appealing for enhanced imaging contrast and minimized dosage.

Interleukin-13 (IL-13), a type 2 cytokine, plays a key role in the host defense such as allergic inflammation via binding to receptors on surfaces of immune and structural cells.[23] IL-13 mediates its effects via a complex receptor system that includes IL-4Rα, IL-13Rα1, and IL-13Rα2.[13–18] IL-13Rα1 and IL-4Rα form a heterodimeric complex that signals through the JAK-STAT pathway. In contrast, IL-13Rα2 has been postulated to be a decoy receptor, not responsible for the signal transduction.[19,20] Increased expression of IL-13Rα2 has been reported to promote tumor progression in glioma and other tumor models[23,24,25] and showed a protective role in a mouse model of cutaneous inflammation.[26] However, the expression of IL-13Rα2 has not been investigated in infectious diseases. Considering its important role in several inflammatory models and the immune system, we hypothesize that this receptor may also be involved in the infection condition and thus can serve as an in vivo biomarker for diagnosis.

In the current study, we aim to utilize a novel class of gadolinium cluster encapsulated metallofullerene ($Gd_3N@C_{80}$) as a MRI contrast agent to detect CPO in mouse tibia via binding to overexpressed IL-13Rα2 receptors in the infection foci. The metallofullerene was functionalized and conjugated to a fragment of IL-13 with optimized coupling conditions to deliver a more homogeneous and bioavailable nanoparticle product, IL-13-TAMRA-$Gd_3N@C_{80}(OH)_{30}(CH_2CH_2\text{-}COOH)_{20}$. This targeted metallofullerene MRI probe specifically bound to lipopolysaccharides (LPS) stimulated macrophages and significantly delineated the hyper-intense MRI signal in the infection foci of the tibia CPO model. Correspondingly, overexpression of IL-13Rα2 receptors were discovered in both LPS-elicited macrophages in vitro and infected tibia. The success of mouse CPO model was also validated.

RESULTS AND DISCUSSION

Characterization of MRI Probe

The XPS survey and multiplex spectra for functionalized fullerene are presented in Figure 1. In the survey XPS spectrum, the peaks centered at 284 and 532 eV are characteristic of the presence of carbon and oxygen species, respectively. In the multiplex spectrum, the C_{1s} peaks, centered at binding energy values of 284.3, 285.6, and 287.4 eV, were assigned to the C—C and C=C, C—O, and C=O, respectively. Based on the peak deconvolution of the XPS profile, the average formula for functionalized fullerene can be described as $Gd_3N@C_{80}(OH)_{30}(CH_2CH_2COOH)_{20}$. In order to enhance the bioavailability and hydrophilicity of the functionalized metallofullerene, we adopted a much longer reaction time (5 days) here allowing a higher derivatization level of hydroxyl and carboxylic groups onto the nanoparticle surface compared to our previous study (2 days).[27]

Determination of the Conjugation Level of IL-13 Peptide per $Gd_3N@C_{80}$

The concentrations of the IL-13 peptide based on the amount of TAMRA dye were determined as followed. Calibration curves of IL-13-TAMRA were constructed using five serial diluted standard solutions and one cosolvent blank at maximum fluorescence emission at 585 nm. Three sample solutions of IL-13-TAMRA-$Gd_3N@C_{80}$−$(OH)_{30}(CH_2CH_2COOH)_{20}$ were fitted in the calibration curve to obtain IL13-TAMRA concentrations (SI Figure 1). Based on triplicate measurements, the average peptide loading (IL-13-TAMRA per $Gd_3N@C_{80}$) was calculated based on molar amounts of IL-13-TAMRA and $[Gd_3N@C_{80}(OH)_{30}(CH_2CH_2–COOH)_{20}]_n$. As shown in Table 1, approximately 1–2 IL-13 peptide units were conjugated per $Gd_3N@C_{80}(OH)_{30}$− $(CH_2CH_2COOH)_{20}$ cage. Compared to the value estimated in our earlier study,[28] the number of IL-13 peptide units per metallofullerene cage in the current study was significantly lower, since we employed a shorter time period (1.5 h versus 12 h) in the conjugation procedure. Our result suggested an improved homogeneity of these nanoparticle samples, which would ultimately reduce the experimental variability in biological tests.

Relaxivity Measurements of the Functionalized $Gd_3N@C_{80}$

The r_1 and r_2 relaxivity results of $[Gd_3N@C_{80}(OH)_{30}(CH_2CH_2COOH)_{20}]_n$ are summarized in Table 2. The nuclear magnetic resonance relaxivity was calculated by the general equation

$$\frac{1}{T_{i,\mathrm{obs}}}=\frac{1}{T_{i,\mathrm{H_2O}}}+\frac{1}{T_{i,\mathrm{para}}}=\frac{1}{T_{i,\mathrm{H_2O}}}+r_i[\mathrm{M}]$$

The observed relaxation rate is determined by both diamagnetic (pure water) and paramagnetic (contrast agent) components. The ratio of paramagnetic relaxation rate to the concentration ([M]) is the relaxivity (r_i) of the paramagnetic compound, which can be experimentally obtained by the slope of $1/T_i$ versus concentrations of the paramagnetic contrast agents.[29] The relaxivity results for f-$Gd_3N@C_{80}$ in Table 2 are lower than previously reported values for similar samples,[28] which were prepared at longer reaction

times and with different hydroxyl content, but are still significantly higher than the commercial contrast agents, Omniscan.

In Vitro MR Contrast Ability of the Functionalized $Gd_3N@C_{80}$ and IL-13-TAMRA-$Gd_3N@C_{80}(OH)_{30}(CH_2CH_2–COOH)_{20}$

In Figure 2, the inversion–recovery images obtained using a clinical 3T MR scanner with 5 mm NMR tubes containing various concentrations of the $[Gd_3N@C_{80}(OH)_{30}–(CH_2CH_2COOH)_2]_n$ and commercial MR contrast agent, Omniscan. The 0.33 μM functionalized metallofullerene and 20 μM Omniscan in water share similar contrast. The contrast ability of IL-13 conjugated MRI probe was demonstrated in an earlier publication.[29] These results show that the functionalized $Gd_3N@C_{80}$ has outstanding contrast relatively to commercial agents.

Increased Expression of IL-13Rα2 Receptors in Macrophages upon LPS Stimulation

IL-13Rα2 has been discovered as a decoy (no signaling) receptor in pathological context involving in type 2 helper T (Th2) cell-driven inflammation, such as asthma.[30–32] It is also among the most extensively studied targets in combating glioblastoma multiform due to its selective expression.[33] However, there has been no report on the expression of IL-13Rα2 in the infectious condition. Monocytes and macrophages are key players in the innate immune system, representing the first line of defense against microorganisms.[34] In this study we employed Raw 264.7 macrophage cell line to detect the expression of IL-13Rα2 upon stimulation with LPS to mimic the inflammatory response during bacterial infection in vitro. Contrary to the low expression in unstimulated macrophages, our immunofluorescence staining results in Figure 3 showed abundant IL-13Rα2 expression after LPS treatment (red fluorescence signal). IgG was used as a negative control. This result indicated a potential role of IL-13Rα2 receptor in the macrophage-associated inflammatory response induced by the infection.

Preferential Probe Binding with Raw 264.7 Cells upon LPS Stimulation

With the built-in feature of TAMRA fluorescence dye on the MRI probe, we further assessed whether escalation of receptor expression on LPS stimulated Raw 264.7 cells could result in higher probe binding. As expected, much stronger TAMRA signal (red fluorescence) was observed in LPS (100 ng/mL, 24 h) stimulated cells compared to unstimulated control cells (Figure 4), predominantly contributed by increased receptor-mediated probe binding after LPS activation. In addition, cell binding studies with a scrambled peptide conjugated $Gd_3N@C_{80}$ suggested Raw 264.7 cells showed little binding in the presence or absence of LPS stimulation (SI Figure 2). The fluorescence signal intensity was quantified and shown in SI Figure 3. Such distinct probe binding data provided us a foundation to proceed into in vivo MRI imaging for differentiation of CPO.

Chronic Post-Traumatic Tibia Osteomyelitis Mouse Model

Given the difficulty in studying *S. aureus* infections in human subjects, animal models serve an integral role in exploring the pathogenesis of osteomyelitis. Mouse has served as the animal of choice to establish disease models, given the superior knowledge of the function

and regulation of their immune system, and their small size, ease of handling, and overall lower cost. However, it is noteworthy that the smaller size makes two-stage revisions and multiple procedures in a single mouse more challenging.[35] To validate our tibia CPO mouse model, longitudinal luminol-bioluminescence imaging and X-ray radiography were employed. Luminol is a redox-sensitive compound that emits blue luminescence when exposed to myeloperoxidase (MPO) generated by recruited neutrophils due to infection. Luminol-bioluminescence imaging at 1.5 weeks showed higher MPO activity in infected tibia compared to the sham (Figure 5A) suggesting more numerous neutrophil infiltration and activation in the acute phase of infection compared to the sham tibia (also see SI Figure 4). Representative X-ray radiographs in Figure 5B showed that all animals experienced evident bone destruction (osteolysis, deformation) and severe inflammatory lesions in those infected tibia after 4 weeks (chronic stage). In addition, clinical signs of illness were apparent during the acute phase of the infection (the first week), such as weight loss (Figure 5C) and decreased mobility of animals due to the initial injury. The gradual recovery in body weight and activity after the first week suggested improving physiological condition of animals during the chronic stage of infection and the infection was only restricted locally in the bacteria inoculated tibia. These data suggested that our surgery was successful and confirmed the progression of CPO and aseptic inflammation developed in separate tibia of the same mouse after trauma.

Histology Confirmed Bone Deformation and Cell Infiltration of Infected Tibia

Histological examination was conducted to visualize the inflammatory response and structural destruction in affected tibiae. After 4 weeks of bacteria inoculation, the infected bones underwent tremendous structural changes during the destruction and remodeling processes. The infected tibia demonstrated massive influx of inflammatory cells accompanied by severe bone tissue destruction such as woven bone, dead bone, and destroyed bone marrow structures (Figure 6, left column). While much less cell infiltration and structural change was detected in the sham tibia (Figure 6, right column). Consistent with the imaging data, bone structural changes in histology confirmed the success of CPO model in mouse tibia and abundant macrophages/monocytes infiltration the chronic osteomyelitis.

Immunohistochemistry Confirmed Overexpression of IL-13Rα2 in Infected Tibia

To corroborate the in vitro findings and MRI results, we employed immunohistochemistry to evaluate IL-13Rα2 expression in both infection and aseptic inflammatory tibia sections. As shown in Figure 7A–C, massive immunopositive cells (brown signal) were detected in chronic stage of tibia infection. In infected sections, these IL-13Rα2 positive cells were primarily observed in regions of infiltrating inflammatory cells in the medullary cavity (Figure 7A,B) and activated osteoblast (Figure 7C). However, only a few immunopositive cells could be located in the medullary cavity of sham tibia (Figure 7D,E), suggesting a low level of IL-13Rα2 expression under aseptic post-traumatic injury. Together with the in vitro cell study and in vivo MRI imaging, these results indicated that IL-13Rα2 would serve as a novel and unique biomarker for detection of differentiation of CPO. In addition, our data would open up a new era of future therapeutic strategy of osteomyelitis, such as IL-13Rα2 targeted therapy and IL-13Rα2-mediated drug retention.

IL-13Rα2 Targeted Hyperintense MRI in the Infection Foci

During both acute and chronic phases of infection, MRI imaging showed hyperintensity on T_1 weighted sequences with the novel IL-13Rα2 targeted probe. As shown in Figure 8A, a single foci was detected in infected tibia during acute phase (1.5 weeks). Repeated MRI during chronic phase (4 weeks post infection) showed a bright signal depicting continuous spreading and expansion of multiple foci of inflammation in the infected tibia (Figure 8B). Interestingly, the longitudinal MRI scan of the same animal revealed a significant change of size and location of the inflammatory foci, suggesting the progression of infectious process in the infected tibia, while no such enhanced signal was observed in sham tibia at both time points. Unlike our targeted probe, a commercially available Gd-based contrast agent Dotarem did not show any hyperintense signal enhancement between pre- and post-contrast images in our model (SI Figure 5). Quantitative analysis of MRI intensity (signal-to-noise ratio, SNR) of this targeted probe was consistent with the visual observation (SI Figure 6). Although future work may be needed to correlate the severity of infection with MRI signal intensity, this proof-of-concept work suggested this novel targeted MRI probe was capable of detecting and differentiating CPO from aseptic inflammation in the current mouse tibia model. In addition, presumably, Gd_3N cluster is stably and securely encapsulated inside the endohedral metallofullerene cage. This unique feature of our probe greatly minimized toxicity concerns associated with free unchelated Gd(III) ions in commonly used MRI contrast agents. Contradictions have been largely reported in patients with impaired renal function because of the risk of nephrogenic systemic fibrosis, as free Gd(III) ions tend to accumulate in the liver, spleen, kidney, and bones and block calcium channels.[2,35] Moreover, our unique metallofullerene nanoparticle structure has been empowered with 25–50-fold more detection sensitivity compared to conventional Gd based contrast agents.[36] Therefore, combined assets of target specificity, minimized toxicity, and improved sensitivity warrant the translational potential of our MRI probe in the clinical differentiation of CPO.

CONCLUSION

In summary, we developed a novel noninvasive imaging approach to detect and differentiate CPO from post-traumatic aseptic inflammation using a novel IL-13Rα2 targeted metallofullerene MRI probe in a mouse tibia model. To the best of our knowledge, we are the first to identify IL-13Rα2 as a unique biomarker for diagnostic imaging of CPO, given to its dramatically increased and distinct expression during bacterial infection. Such a translational imaging approach would eventually aid clinical differentiation of CPO from aseptic post-traumatic or surgical inflammation, hence providing critical and timely information for decision making of therapeutic strategy.

EXPERIMENTAL SECTION

Chemical Materials

$Gd_3N@C_{80}$ was purchased from LUNA Innovations (Danville, VA). The TAMRA-VDKL-LLHLKKLFREGQFNREGQFNRNFESIIICRDRT-OH (IL-13-TAMRA peptide), a shorter active peptide for IL-13Rα2 receptor sites, was purchased from New England Peptide LLC (Gardner, MA). Gibco Dulbecco's Modified Eagle Medium (high glucose 4.5 g/L)

(DMEM), fetal bovine serum (FBS), and Prolong Gold antifade mountant with DAPI were purchased from Life Technologies (Grand Island, NY). Dulbecco's phosphate-buffered saline (DPBS), and penicillin-streptomycin were purchased from Gibco Invitrogen (Carlsbad, CA). Other chemicals, such as 2-(*N*-morpholino)-ethanesulfonic acid (MES), 1-ethyl-3-(3-(dimethylamino)-propyl) carbodiimide (EDC), and *N*-hydroxysulfosuccinimide (Sulfo-NHS) were obtained from Sigma-Aldrich (St. Louis, MO) unless mentioned.

Conjugation of IL-13-TAMRA-$Gd_3N@C_{80}(OH)_{30}-(CH_2CH_2COOH)_{20}$

The elaboration of the carboxyl group onto the cage surface of $Gd_3N@C_{80}$ was performed using an improved procedure from our earlier studies.[27] Briefly, 10 mg of the metallofullerene, $Gd_3N@C_{80}$, and 8 mg succinic acid acyl peroxide (5 equiv) were dissolved in 10 mL of 1,2-dichlorobenzene (Scheme 1). The resultant solution was deoxygenated with flowing argon and heated at 84 °C for 5 days. Additional succinic acid acyl peroxide (5 equiv) was added every 12 h. After the reaction, 8 mL of 0.2 M NaOH was added to extract the water-soluble product. The top layer was concentrated, and the residue was purified by a Sephadex G-25 size-exclusion gel column.[27]

A volume of 500 μL of fullerene surface carboxylated $Gd_3N@C_{80}$ was dissolved in MES (pH = 5.3) solution, then filtered through a 0.45 μm syringe filter. The carboxyl groups were activated by 70 μL of 0.5 M EDC and the same amount of Sulfo-NHS. After 10 min, 85 μL of the IL-13-TAMRA peptide (dissolved in DMSO, 2 mg/mL) was added, vortexed, and incubated at room temperature for 1.5 h. Then, 70 μL of 0.5 M hydroxylamine solution was introduced to quench the reaction. The resulting solution was filtered through Zeba-brand spin columns at a rate of 5000 rpm for 2 min. The receptacle portion of the spin column was thoroughly rinsed to ensure that all the product was removed from the column.[28,29]

Characterization of Functionalized $Gd_3N@C_{80}$ with IL-13 Peptide Loading Per Fullerene

The functionalized metallofullerene was characterized by XPS to measure the elemental composition and empirical formula. To determine the loading of IL-13 peptide per fullerene cage, a calibration curve was constructed by diluting a stock solution of IL-13-TAMRA in DMSO/water. Stock solutions of functionalized metallofullerene conjugated with IL-13-TAMRA were prepared in the same cosolvent. The concentration of functionalized $Gd_3N@C_{80}$ was measured by ICP-MS. IL-13-TAMRA standards and IL-13-TAMRA-functionalized $Gd_3N@C_{80}$ samples were transferred into a black Costar 96-well plate, after which fluorescence was measured in Cytation3 Cell Imaging Multi-Mode Reader (excitation 550 nm, emission 585 nm, gain 120, optics on the bottom, xenon flash light source, 100 ms delay).

Relaxivity Measurements of the Functionalized $Gd_3N@C_{80}$

The T_1 and T_2 relaxation times were measured on Bruker Minispec mq 20 (0.47 T), mq 60 (1.41 T) analyzers. The inversion–recovery method was used to measure the spin–lattice relaxation time T_1, and the Carr–Pucell–Meiboom–Gill (CPMG) method was used for the spin–spin relaxation time T_2 measurement. Errors in T_1 and T_2 values were less than ±2%.

In Vitro MRI Study of the Functionalized $Gd_3N@C_{80}$

The in vitro inversion–recovery MR images were obtained under a 3T clinical scanner for the visual confirmation of the efficiency of the functionalized fullerene working as a contrast agent. Various concentrations of the Gd based fullerenes, and the commercial contrast agent Omniscan were used and compared.

Raw 264.7 Cell Culture, Immunofluorescence Staining, and Probe Binding

Raw 264.7 cells were cultured in complete growth medium (DMEM + 10% FBS + 1% Penicillin/Streptomycin) at 37 °C with 5% CO_2. One day before the experiment, cells were seeded onto sterile coverslips in a 6-well plate at a density of 4×10^5 cells/mL and incubated overnight. Then cells were treated with or without LPS (100 ng/mL) for 24 h in serum-free media.

For immunofluorescence staining,[37] cells on coverslips were fixed with 4% paraformaldehyde for 30 min. Goat anti-mouse IL-13Rα2 antibody (1:5000) was used to detect IL-13Rα2, and followed by incubation with Alexa Fluo 594 chicken anti-goat secondary antibody, (1:5000, Invitrogen, Waltham, MA) for 30 min. IgG control was performed excluding the primary antibody incubation. Cell nuclei were countered stained with DAPI.

For probe binding experiments, cells treated with or without LPS were fixed with 4% paraformaldehyde for 30 min and incubated with 1 μM IL-13-functionalized $Gd_3N@C_{80}$ MRI probe labeled with TAMRA and washed with PBS twice. Cell nuclei were counterstained with DAPI. Fluorescence images were taken with a fluorescence microscope (LSM 510-UV, Carl Zeiss, Germany) and processed by NIS Element Basic Research software (Nikon Instruments Melville, NY) with the exact same setting for infected and sham tibia samples following our published protocols.[38]

CPO Mouse Model

Animal protocol was approved by the Institutional Animal Care and Use Committee at the University of Virginia. *S. aureus* ATCC 25923 (ATCC, VA) cultivated overnight in terrific broth medium at room temperature. Balb/C mice (8–10 weeks old, female, 20–25 g, Envigo) were maintained in a 12 h light cycle vivarium facility. 5-mm-long Vicryl suture (#2–0) were soaked in 1×10^7 CFU/mL (150 μL) or saline (150 μL) for 30 min, and a hole was developed by a 27G needle in the proximal end of the tibia, followed by inserting bacteria (right) or PBS (left) soaked suture intramedullary ($n = 5$). Body weights were continuously monitored during the experimental period.

Luminol-Bioluminescence Imaging of Myeloperoxidase

At 1.5 weeks post-infection, bioluminescence imaging was performed at 20 min after intraperitoneal injection of luminol solution (200 μL, 5 mg/100 μL in DMSO) on Xenogen IVIS Spectrum (PerkinElmer, CA) and processed on Live Image software (PerkinElmer) with open filter and exposure time of 60 s.[16]

In Vivo MRI Study of IL-13-TAMRA-$Gd_3N@C_{80}$ Probe

In vivo MRI was acquired at a 7 T ClinScan Bruker/Siemens MR scanner (Bruker, Billerica, MA) at 1.5 and 4 weeks after bacterial inoculation. Immediately before the scan, probe IL-13-functionalized $Gd_3N@C_{80}$ (4 nmol per 20 g body weight) or commercially available contrast agent Dotarem (50 nmol per 20 g body weight) (Guerbet, Bloomington, IN) was administered intravenously into mice. Animals were anesthe-tized with 1.5% isoflurane during the procedure. Tibiae were imaged by T_1 weighted images with following settings: T_1 (Spin–Echo)-Voxel size 0.102 × 0.102 × 0.7 mm^3, T_R 600 ms, T_E 11 ms, Averages 3, Slice Thickness of 0.7 mm, matrix 256 × 256; MR images were segmented using Siemens Syngo FastView (Siemens Medical Solutions, Malvern, PA).[15]

X-ray Radiography

Immediately after the last MRI scan at 4 weeks post infection, mice were euthanized by CO_2 asphyxiation. X-ray radiograph was captured using a low-energy X-ray (Faxitron, Model 43805N, OR) with an exposure time of 30 s (30 kV). X-ray films were then processed in Konica Minolta SRX-101A Tabletop Processor (Konica Minolta Business Solutions, Ramsey, NJ).[39]

Histological and Immunohistochemical Staining

Mouse tibiae were dissected and fixed in 10% formalin for 3 days, decalcified in 0.25 M EDTA for 2 weeks, embedded in paraffin, and sectioned into 5 μm thickness. Hematoxylin and eosin (H/E) staining was performed following standard protocols.[40,41] To confirm expression of IL-13Rα2 after infection and traumatic surgery, immunohistochemical staining was performed following our previously published protocols.[42] Briefly, tibia sections were deparaffinized, rehydrated, and treated with 3% hydrogen peroxide in methanol for 30 min for blockade of endogenous peroxidase and followed by antigen retrieval in 10 mM citrate buffer (pH 6.0) for 30 min in 85 °C water bath. Sections were then incubated with goat antimouse IL-13Rα2 antibody (1:5000, R&D Systems, Minneapolis, MN) overnight at 4 °C, and followed by secondary biotinylated horse antigoat IgG antibody (1:200, Vector Laboratories, Burlingame, CA).

Statistical Analysis

All in vitro experiments were performed at least in triplicate and data were presented as mean ± STDEV. Data comparing two groups were analyzed with a Student's *t*-test. A *p*-value of less than 0.05 was considered statistically significant.

Supplementary Material

Refer to Web version on PubMed Central for supplementary material.

Acknowledgments

We are grateful to financial support from Orthopaedic Trauma Association and partially from National Institute of Health NIAMS R01AR064792. We also appreciate the technical assistance of Molecular Imaging Core and Research Histology Core at University of Virginia.

References

1. Horst SA, Hoerr V, Beineke A, Kreis C, Tuchscherr L, Kalinka J, Lehne S, Schleicher I, Köhler G, Fuchs T, et al. A Novel Mouse Model of Staphylococcus aureus Chronic Osteomyelitis That Closely Mimics the Human Infection. Am J Pathol. 2012; 181:1206–1214. [PubMed: 22902429]
2. Lew DP, Waldvogel FA. Osteomyelitis. N Engl J Med. 1997; 336:999–1007. [PubMed: 9077380]
3. Kamat AS. Infection Rates in Open Fractures of the Tibia: Is the 6-h Rule Fact or Fiction? Ad Orthop. 2011; 2011:4.
4. Kurtz S, Ong K, Lau E, Mowat F, Halpern M. Projections of Primary and Revision Hip and Knee Arthroplasty in the United States from 2005 to 2030. J Bone Joint Surg. 2007; 89:780–785. [PubMed: 17403800]
5. Lew DP, Waldvogel FA. Osteomyelitis. Lancet. 2004; 364:369–379. [PubMed: 15276398]
6. Mader JT, Norden C, Nelson JD, Calandra GB. Evaluation of new anti-infective drugs for the treatment of osteomyelitis in adults. Clin Infect Dis. 1992; 15:S155. [PubMed: 1477223]
7. Zuluaga AF, Galvis W, Jaimes F, Vesga O. Lack of microbiological concordance between bone and non-bone specimens in chronic osteomyelitis: an observational study. BMC Infect Dis. 2002; 2:8. [PubMed: 12015818]
8. Perry CR, Pearson RL, Miller GA. Accuracy of cultures of material from swabbing of the superficial aspect of the wound and needle biopsy in the preoperative assessment of osteomyelitis. J Bone Joint Surg Am. 1991; 73:745–9. [PubMed: 2045400]
9. Khatri G, Wagner DK, Sohnle PG. Effect of bone biopsy in guiding antimicrobial therapy for osteomyelitis complicating open wounds. Am J Med Sci. 2001; 321:367–71. [PubMed: 11417751]
10. Lee YJ, Sadigh S, Mankad K, Kapse N, Rajeswaran G. The imaging of osteomyelitis. Quant Imaging Med Surg. 2016; 6:184–198. [PubMed: 27190771]
11. Palestro CJ. Radionuclide Imaging of Musculoskeletal Infection: A Review. J Nucl Med. 2016; 57:1406–1412. [PubMed: 27390160]
12. Govaert GAM, Glaudemans AWJM. Nuclear medicine imaging of posttraumatic osteomyelitis. Eur J Trauma Emerg Surg. 2016; 42:397–410. [PubMed: 26886235]
13. Xiao L, Zhang Y, Berr SS, Chordia MD, Pramoonjago P, Pu L, Pan D. A novel near-infrared fluorescence imaging probe for in vivo neutrophil tracking. Mol Imaging. 2012; 11:372–82. [PubMed: 22954181]
14. Xiao L, Zhang Y, Liu Z, Yang M, Pu L, Pan D. Synthesis of the Cyanine 7 labeled neutrophil-specific agents for noninvasive near infrared fluorescence imaging. Bioorg Med Chem Lett. 2010; 20:3515–7. [PubMed: 20488705]
15. Xiao L, Zhang Y, Yang Z, Xu Y, Kundu B, Chordia MD, Pan D. Synthesis of PECAM-1-specific 64Cu PET imaging agent: Evaluation of myocardial infarction caused by ischemia-reperfusion injury in mouse. Bioorg Med Chem Lett. 2012; 22:4144–4147. [PubMed: 22578454]
16. Zhang Y, Xiao L, Chordia MD, Locke LW, Williams MB, Berr SS, Pan D. Neutrophil Targeting Heterobivalent SPECT Imaging Probe: cFLFLF-PEG-TKPPR-99mTc. Bioconjugate Chem. 2010; 21:1788–1793.
17. Locke LW, Chordia MD, Zhang Y, Kundu B, Kennedy D, Landseadel J, Xiao L, Fairchild KD, Berr SS, Linden J, Pan D. A novel neutrophil-specific PET imaging agent: cFLFLFK-PEG-64Cu. J Nucl Med. 2009; 50:790–7. [PubMed: 19372473]
18. Pugmire BS, Shailam R, Gee MS. Role of MRI in the diagnosis and treatment of osteomyelitis in pediatric patients. World J Radiol. 2014; 6:530–537. [PubMed: 25170391]
19. Neuwelt A, Sidhu N, Hu CAA, Mlady G, Eberhardt SC, Sillerud LO. Iron-Based Superparamagnetic Nanoparticle Contrast Agents for MRI of Infection and Inflammation. AJR, Am J Roentgenol. 2015; 204:W302–W313. [PubMed: 25714316]
20. Bierry G, Jehl F, Boehm N, Robert P, Dietemann JL, Kremer S. Macrophage imaging by USPIO-enhanced MR for the differentiation of infectious osteomyelitis and aseptic vertebral inflammation. Eur Radiol. 2009; 19:1604–1611. [PubMed: 19198846]

21. Faz-Lopez B, Morales-Montor J, Terrazas LI. Role of Macrophages in the Repair Process during the Tissue Migrating and Resident Helminth Infections. BioMed Res Int. 2016; 2016:8634603. [PubMed: 27648452]
22. Resnick M, Fibach E, Lebastard M, Levy L, Bercovier H. Response of the murine hematopoietic system to chronic infection with Mycobacterium lepraemurium. Infect Immun. 1988; 56:3145–3151. [PubMed: 3053453]
23. Wills-Karp M, Luyimbazi J, Xu X, Schofield B, Neben TY, Karp CL, Donaldson DD. Interleukin-13: Central Mediator of Allergic Asthma. Science. 1998; 282:2258–2261. [PubMed: 9856949]
24. Sengupta S, Thaci B, Crawford AC, Sampath P. Interleukin-13 Receptor Alpha 2-Targeted Glioblastoma Immunotherapy. BioMed Res Int. 2014; 2014:952128. [PubMed: 25247196]
25. Li T, Dorn HC. Biomedical Applications of Metal-Encapsulated Fullerene Nanoparticles. Small. 2016; doi: 10.1002/smll.201603152
26. Sivaprasad U, Warrier MR, Gibson AM, Chen W, Tabata Y, Bass SA, Rothenberg ME, Khurana Hershey GK. IL-13Rα2 Has a Protective Role in a Mouse Model of Cutaneous Inflammation. J Immunol. 2010; 185:6802–6808. [PubMed: 20971924]
27. Shu CY, Corwin FD, Zhang JF, Chen ZJ, Reid JE, Sun MH, Xu W, Sim JH, Wang CR, Fatouros PP, et al. Facile Preparation of a New Gadofullerene-Based Magnetic Resonance Imaging Contrast Agent with High H-1 Relaxivity. Bioconjugate Chem. 2009; 20:1186–1193.
28. Fillmore HL, Shultz MD, Henderson SC, Cooper P, Broaddus WC, Chen ZJ, Shu CY, Zhang JF, Ge JC, Dorn HC, et al. Conjugation of functionalized gadolinium metallofullerenes with IL-13 peptides for targeting and imaging glial tumors. Nanomedicine. 2011; 6:449–458. [PubMed: 21542684]
29. Li TH, Murphy S, Kiselev B, Bakshi KS, Zhang JY, Eltahir A, Zhang YF, Chen Y, Zhu J, Davis RM, et al. A New Interleukin-13 Amino-Coated Gadolinium Metallofullerene Nanoparticle for Targeted MRI Detection of Glioblastoma Tumor Cells. J Am Chem Soc. 2015; 137:7881–7888. [PubMed: 26022213]
30. Alizadeh-Navaei R, Rafiei A, Hedayatizadeh-Omran A, Mohammadzadeh I, Arabi M. Gene Susceptibility in Iranian Asthmatic Patients: A Narrative Review. Ann Med Health Sci Res. 2014; 4:837–840. [PubMed: 25506473]
31. Vatrella A, Fabozzi I, Calabrese C, Maselli R, Pelaia G. Dupilumab: a novel treatment for asthma. J Asthma Allergy. 2014; 7:123–130. [PubMed: 25214796]
32. Bice JB, Leechawengwongs E, Montanaro A. Biologic targeted therapy in allergic asthma. Ann Allergy, Asthma, Immunol. 2014; 112:108–115. [PubMed: 24468249]
33. Feuerstein R, Kolter J, Henneke P. Dynamic interactions between dermal macrophages and Staphylococcus aureus. J Leukocyte Biol. 2017; 101:99. [PubMed: 27733573]
34. Reizner W, Hunter JG, O'Malley NT, Southgate RD, Schwarz EM, Kates SL. A systematic review of animal models for Staphylococcus aureus osteomyelitis. Eur Cell Mater. 2014; 27:196–212. [PubMed: 24668594]
35. Khawaja AZ, Cassidy DB, Al Shakarchi J, McGrogan DG, Inston NG, Jones RG. Revisiting the risks of MRI with Gadolinium based contrast agents–review of literature and guidelines. Insight Imaging. 2015; 6:553–558.
36. Murphy SV, Hale A, Reid T, Olson J, Kidiyoor A, Tan J, Zhou Z, Jackson J, Atala A. Use of trimetasphere metallofullerene MRI contrast agent for the non-invasive longitudinal tracking of stem cells in the lung. Methods. 2016; 99:99–111. [PubMed: 26546729]
37. Xiao L, Ding M, Saadoon O, Vess E, Fernandez A, Zhao P, Jin L, Li X. A novel culture platform for fast proliferation of human annulus fibrosus cells. Cell Tissue Res. 2016; doi: 10.1007/s00441-016-2497-4
38. Xiao L, Ding M, Zhang Y, Chordia M, Pan D, Shimer A, Shen F, Glover D, Jin L, Li X. A Novel Modality for Functional Imaging in Acute Intervertebral Disk Herniation via Tracking Leukocyte Infiltration. Mol Imaging Biol. 2017; doi: 10.1007/s11307-016-1038-6
39. Liang H, Wang K, Shimer AL, Li X, Balian G, Shen FH. Use of a bioactive scaffold for the repair of bone defects in a novel reproducible vertebral body defect model. Bone. 2010; 47:197–204. [PubMed: 20580872]

40. Jin L, Wan Y, Shimer AL, Shen FH, Li XJ. Intervertebral disk-like biphasic scaffold–demineralized bone matrix cylinder and poly(polycaprolactone triol malate) –for interbody spine fusion. J Tissue Eng. 2012; 3:204173.

41. Jin L, Feng G, Reames DL, Shimer AL, Shen FH, Li X. The Effects of Simulated Microgravity on Intervertebral Disc Degeneration. Spine J. 2013; 13:235–242. [PubMed: 23537452]

42. Jin L, Liu Q, Scott P, Zhang D, Shen F, Balian G, Li X. Annulus Fibrosus Cell Characteristics Are a Potential Source of Intervertebral Disc Pathogenesis. PLoS One. 2014; 9:e96519. [PubMed: 24796761]

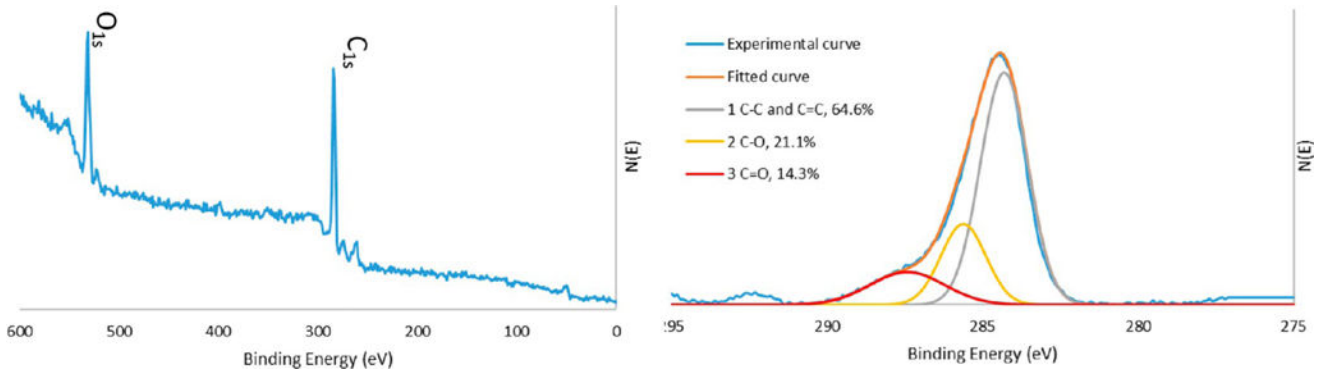

Figure 1.

XPS survey (left) and multiplex (right) spectral regions of $Gd_3N@C_{80}(OH)_{30}(CH_2CH_2COOH)_{20}$.

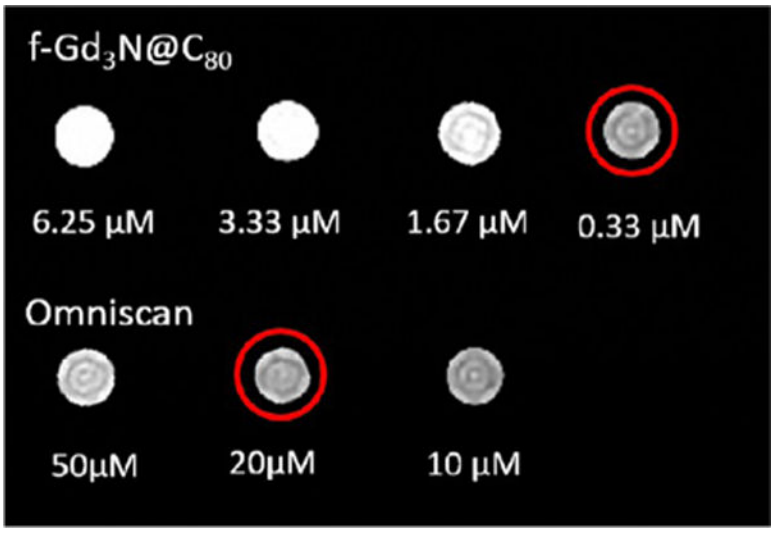

Figure 2.

Inversion–recovery MR images (T_1 = 1000 ms, T_R = 5000 ms, T_E = 30 ms) with f-$Gd_3N@C_{80}$ and Omniscan as contrast agent. Top row from right to left: 0.33, 1.67, 3.33, and 6.25 μM f-$Gd_3N@C_{80}$ in water. Bottom row from right to left: 10, 20, and 50 μM commercial agent in water. The 0.33 μM f-$Gd_3N@C_{80}$ and 20 μM Omniscan in water exhibit comparable contrast.

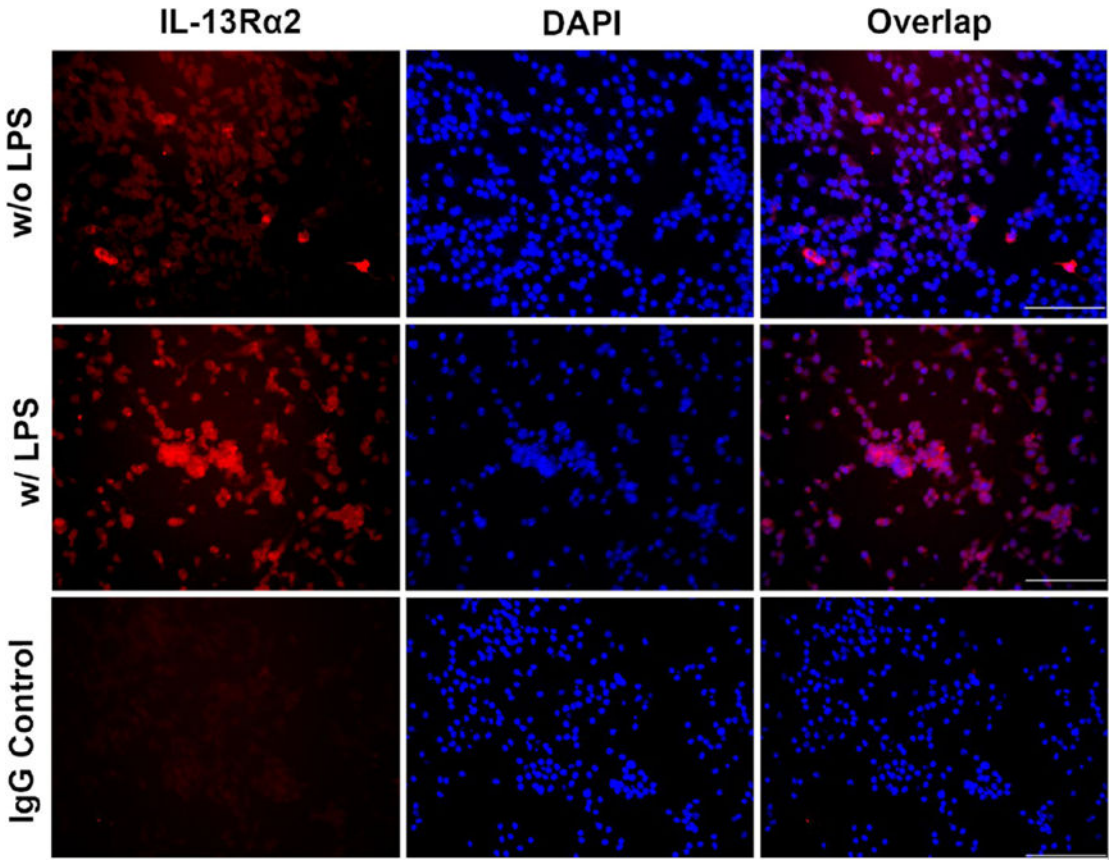

Figure 3.

Immunofluorescence staining of IL-13Rα2 in Raw 264.7 cells with or without LPS (100 ng/mL) treatment for 1 day. Increased expression of IL-13Ra2 (red fluorescence) was observed in the cytosol upon LPS stimulation (middle row) compared to nontreated (upper row) and IgG controls (lower row). Scale bar represented 100 μm.

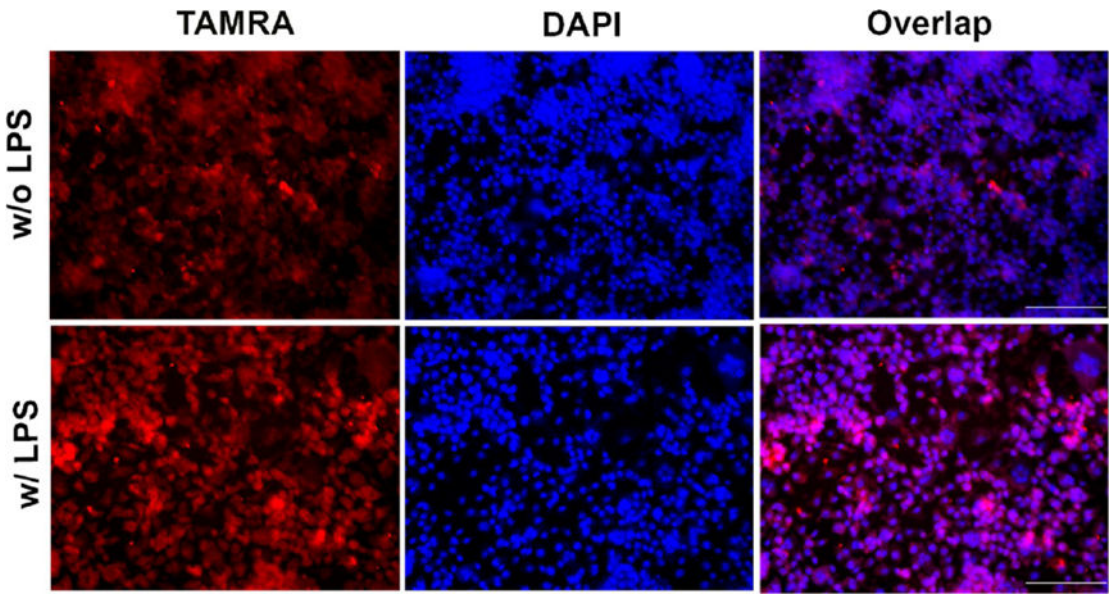

Figure 4.

In vitro probe binding with Raw 264.7 cells with or without LPS (100 ng/mL) treatment for 1 day. TAMRA-tagged MRI probe (1 μM) was incubated with cells for 30 min at room temperature. Much higher cell-bound TAMRA (red) fluorescence signal was observed in LPS-treated cells (lower row) compared to nontreated cells (upper row), suggesting more probe binding with Raw 264.7 cells upon LPS stimulation. Scale bar represented 100 μm.

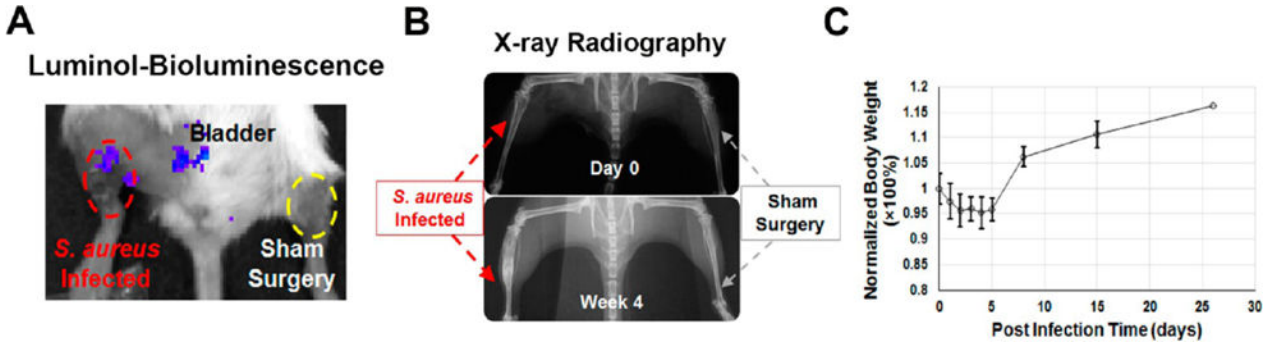

Figure 5.

Infection parameters during the course of chronic post-traumatic tibia osteomyelitis. (A) Luminol-bioluminescence imaging showed higher myeloperoxidase activity in infection compared to sham. (B) X-ray radiograph demonstrated severe bone deformation and inflammatory lesion in infected tibia compared to sham. (C) Local infection was confirmed via continuous monitoring of body weight up to 4 weeks post infection.

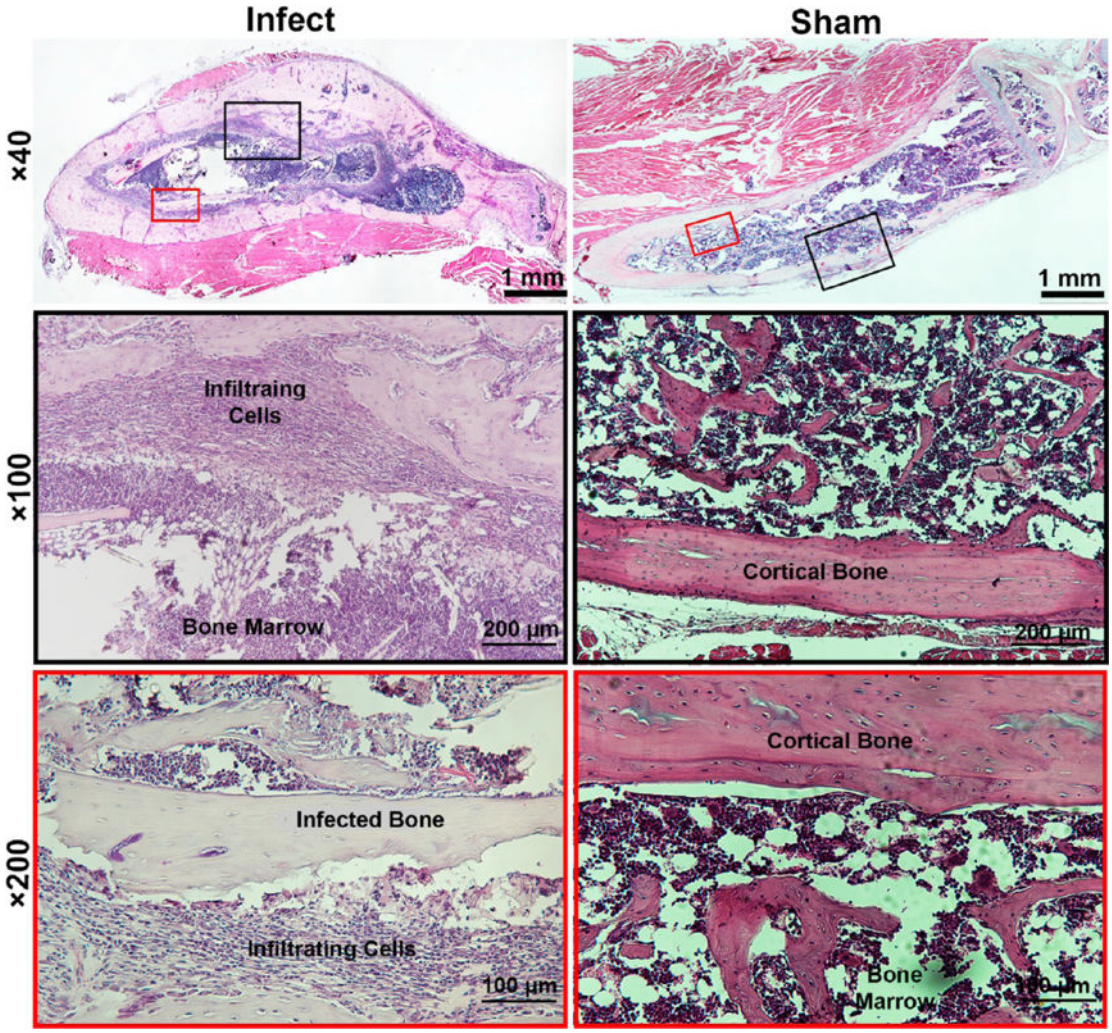

Figure 6.

Hematoxylin and eosin staining of infected (left column) and sham tibia (right column) after 4 weeks post infection. Low magnification images (upper row) depicted overall structural change in the infected tibia was much more severe than the sham. High magnification images in mid-(×100) and lower-rows (×200) showed massive infiltration of inflammatory cells and formation of dead bones inside the medullary cavity of infected tibia while almost few infiltrated cells and much milder bone deformation was observed in the sham tibia.

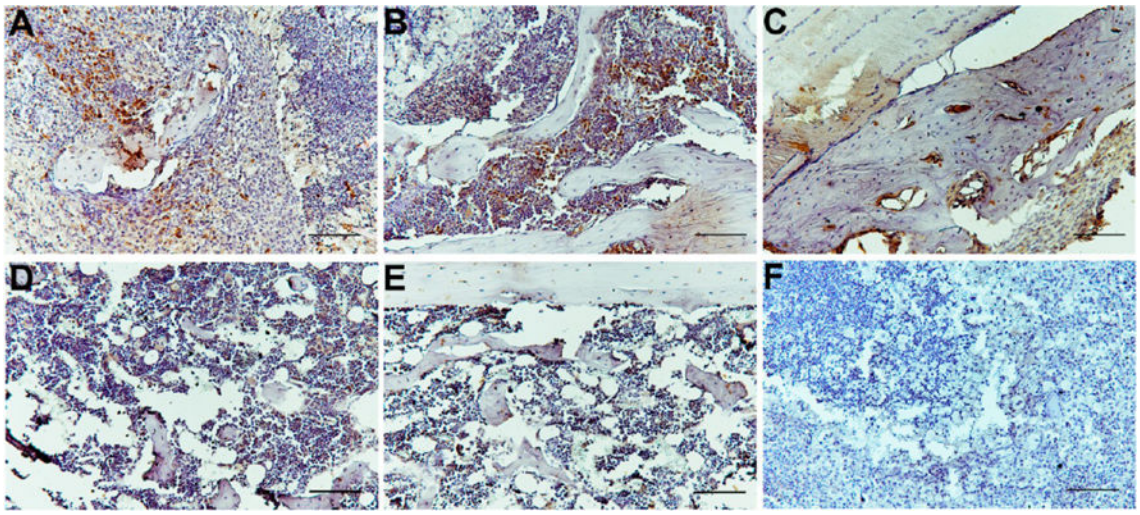

Figure 7.

Immunohistochemical staining of IL-13Rα2 expression in mouse tibia after 4 weeks of *S. aureus* induced infection. In the infected tibia, a significant amount of IL-13Rα2 immunopositive signal (brown cells) was primarily detected in the medullary cavity where massive infiltrating cells (A) and infected bone marrow (B) located. Some immunopositive signal was also observed in activated osteoclasts in the cortical bone of infected tibia (C). In comparison, few positively stained cells could be detected in either bone marrow (D) or cortical bone (E) of sham tibia. IgG control staining of infected sample (F) resulted in no positive signal suggesting the specificity of the procedure. All images were taken at ×200 magnification. Scale bar represented 100 μm.

Figure 8.

Representative T_1-weighted (Spin–Echo, T_R 600 ms, T_E 11 ms) MRI images of infected and sham tibia after intravenous injection of probe IL-13-$Gd_3N@C_{80}(OH)_{30}(CH_2CH_2COOH)_{20}$ (4 nmol per 20 g mice) at 1.5 (A) and 4 weeks (B) post-infection. Yellow arrows indicated hyperintensity of MRI signal in infected foci while white arrowheads suggested the contralateral sham tibia subjected to traumatic procedure. Interestingly, longitudinal MRI scan of the same animal revealed a significant change of size and location of the inflammatory foci in the infected tibia, suggesting the progression of osteomyelitis (yellow arrows).

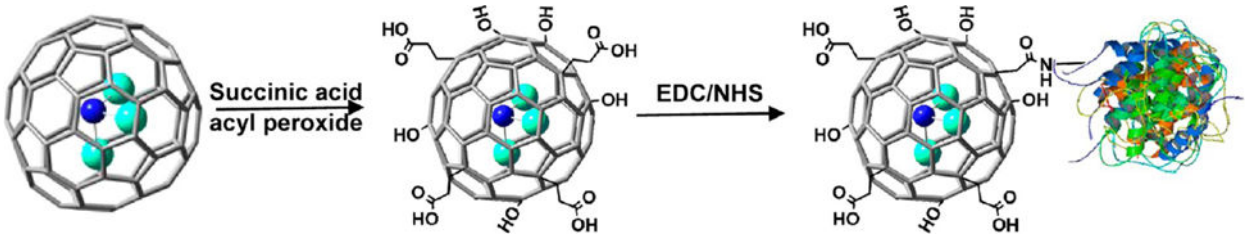

Scheme 1.

Functionalization and Conjugation Process of IL-13-TAMRA-$Gd_3N@C_{80}(OH)_{30}(CH_2CH_2COOH)_{20}$ (Gray, Carbon; Aqua, Gadolinium Ion; Blue, Nitrogen)

Table 1

Concentration of the IL-13-TAMRA, and Functionalized $Gd_3N@C_{80}$ (per Cage)

	Intensity of IL-13-TAMRA-f-$Gd_3N@C_{80}$	**Conc of IL-13-TAMRA (μM)**	**Conc of f-$Gd_3N@C_{80}$ (μM)**	**Peptide loading of per f-$Gd_3N@C_{80}$**
Sample 1	10157	1.58	1.08	1.40
Sample 2	17145	2.66	1.62	1.64
Sample 3	24405	3.79	2.70	1.46

Table 2

Relaxivities of Functionalized Gadolinium Metallofullerenes (Units of mM^{-1} s^{-1} per mM in Pure Water at 25 °C)

	R_1 relaxivity (mM^{-1} s^{-1})		R_2 relaxivity (mM^{-1} s^{-1})	
contrast agents	**0.47 T**	**1.41 T**	**0.47 T**	**1.41 T**
f-$Gd_3N@C_{80}$ (2–100 μM)	91	118	110	145
Omniscan	~4	~4	~4	~4